Available online at www.sciencedirect.com
ScienceDirect
Journal of Sound and Vibration 321 (2009) 1144–1170
JOURNAL OF SOUND AND VIBRATION
www.elsevier.com/locate/jsvi

Empirical mode decomposition, an adaptive approach for interpreting shaft vibratory signals of large rotating machinery

Wenxian Yang[a,b,*], P.J. Tavner[a]

[a]*New and Renewable Energy Group, School of Engineering, Durham University, Durham DH1 3LE, UK*
[b]*Institute of Vibration Engineering, Northwestern Polytechnical University, Xi'an 710072, PR China*

Received 17 October 2007; received in revised form 29 September 2008; accepted 8 October 2008
Handling Editor: C.L. Morfey
Available online 30 November 2008

Abstract

The Fourier transform (FT) has been the most popular method for analyzing large rotating machine shaft vibration problems, but it assumes that these vibration signals are linear and stationary. However, in reality this is not always true. Nonlinear and non-stationary shaft vibration signals are often encountered during the start-up and shut-down processes of the machines. Additionally, mechanical faults, for example rotor-to-stator rubbing, fluid excitation, part-loosening, and shaft cracking, are nonlinear. Owing to these reasons, an accurate analysis of shaft vibration cannot always be achieved by using the FT.

An alternative tool, the wavelet transform (WT), is now being used to improve the situation. But the efficiency is a problem especially when applying the WT to the accurate analysis of a large-scale, lengthy data.

In view of the powerful capability of empirical mode decomposition (EMD) to process nonlinear/non-stationary signals, its algorithm efficiency and its satisfactory performance in minimizing energy leakage, the EMD is used in this paper to analyze the problem, the signals investigated are adaptively decomposed into a finite number of intrinsic mode functions (IMFs). The principal IMFs, identified using an energy-distribution threshold, dominate the signals' oscillation. So, 'purified' shaft vibration signals can be reconstructed from these principal IMFs. To remove interference present in principal IMFs, an adaptive band-pass filter is designed, whose central frequency is automatically set to the frequency dominating the IMF being investigated. To facilitate the observation of transient shaft vibration, a transient shaft orbit (TSO) is constructed by introducing timescale into the orbit drawing process. Nine mathematical criteria are also proposed to evaluate the shaft vibrations exhibited in the IMFs and TSOs. The novelty of this approach is that the EMD provides an adaptive, effective, and efficient way to obtain 'purified' shaft vibration signals, which describe the transient shaft vibration more vividly and precisely, reducing misinterpretation of the machine running condition.

The approach is validated by two practical examples:

- Part-loosening incident on a large centrifugal compressor.
- Fluid excitation incident on a centrifugal compressor.

Calculations of the mathematical criteria for seven different running conditions of these large rotating machines are also presented.

*Corresponding author at: New and Renewable Energy Group, School of Engineering, Durham University, Durham DH1 3LE, UK.
E-mail address: wenxian.yang@durham.ac.uk (W. Yang).

0022-460X/$ - see front matter
doi:10.1016/j.jsv.2008.10.012

It is demonstrated that the proposed technique provides a feasible and reliable way to interpret shaft vibration, by which means the machine condition can be diagnosed correctly.

1. Introduction

Shaft vibration signals, especially shaft orbit measured by two perpendicularly mounted displacement probes, carry abundant and vital dynamic information for condition monitoring large rotating machinery [1–3], through which potentially harmful malfunctions may be isolated and identified [4,5]. A review of the literature published in the last two decades reveals that two main approaches, the Fourier and wavelet transforms (FT and WT), are popular for processing large rotating machine shaft vibration signals.

Advanced FT-based techniques were developed for shaft vibration signals following the establishment of the mathematical basis of the Holospectrum [6] and reinforced recently by Shi et al. [1], who improved the algorithm for calculating signal amplitude, frequency, and phase information using the high-resolution spectrum (HRS).

In the last two decades, FT-based techniques have been widely adopted, for example, Chen et al. [7] adopted this approach to extract integrated vibration information from rotating machines; Yang et al. used this approach to diagnose a shaft with a transverse crack [8] and investigated the factors which influence the transient vibration of the shaft [9]. However, due to the averaging effect, the FT-based techniques are still not very suitable to deal with nonlinear/non-stationary signals despite efforts to improve them [1,10].

In view of this, the WT has been used as an alternative for depicting the transient vibration of the machine. For example, Li [2] adopted the harmonic wavelet packets decomposition method to obtain the shaft orbit created by the sub-frequency signal and Zhang et al. [3] tried diagnosing a hydropower generator with the aid of the WTs. A similar approach was also employed by Chen [4] and Peng et al. [5] to diagnose rotating machines. But this does not mean that the WT-based techniques are perfect in all applications. In fact, sometimes they suffer from intensive calculations especially when they are applied to processing large-scale, lengthy data. Energy leakage occurring in the vicinity of frequencies of interest cannot be avoided by them due to the limited length of wavelet function and the frequency band overlap between the quadrature mirror filters [11,12]. As a consequence, the smeared time–frequency spectrum inevitably gives rise to signal interpretation difficulties [13,14].

The empirical mode decomposition (EMD), attributed to provide a more realistic signal representation, without artifacts imposed by the non-adaptive limitations of the FT and the WT, has recently been regarded as a powerful tool for analyzing nonlinear/non-stationary signals. The EMD possesses high efficiency in computation [15,16], because it allows a direct algorithmic analysis of the signal time waveform, enabling it to deal with large-scale, lengthy data. Moreover, the EMD is an adaptive, non-constrained decomposition of the signal into a finite number of intrinsic mode functions (IMFs). Each IMF represents one simple oscillatory signal mode. In comparison with the WT the EMD does not show serious energy leakage problem in the vicinity of frequencies of interest [17]. These advantages allow the EMD to be a more powerful and promising tool for solving condition monitoring problems associated with nonlinear/non-stationary signal analysis [18–22]. However, like other signal processing methods the EMD also suffers from problems, for example the end effect considered in Refs. [23–25] and the disturbances due to pseudo-information at low frequencies [26,27]. But, as reported in the literature, these defects can be overcome by taking measures in the calculation of the EMD.

In this paper, the EMD is employed to analyze the transient vibration of the shafts of large rotating machines. The novelties of this application may be summarized in the following three points:

- The local-adaptive and energy-conservation decomposition is introduced to analyze the transient shaft vibration. This is very helpful to detect those incipient faults and insignificant changes of machine running condition.

- The EMD has an efficient computing algorithm and does not suffer from the inherent shortcomings in the FT and WT, allowing the EMD to obtain the 'purified' shaft vibration signal '*truly*' and '*quickly*'.
- The EMD is able to process massive data efficiently, it enables to monitor and diagnose shaft vibration for a longer period of time. This is definitely helpful for further guaranteeing the correctness of the diagnosis and assessment of machine running condition.

To further strengthen the power of EMD-based condition monitoring and fault diagnosis for rotating machines, a new concept namely the transient shaft orbit (TSO) is constructed using those principal IMFs and nine mathematical criteria will be proposed for quantitatively assessing shaft vibration. More details about these techniques will be given in later sections.

It should be noted that all the vibration data presented in this paper were collected from real centrifugal compressors with similar rotor-bearing systems operating in Shijiazhuang Petroleum Plant, Xingjiang Petroleum-Chemical Plant, and ZhenHai Oil Refinery in China and the data were collected and managed by the Research Institute of Diagnostics and Cybernetics in Xian Jiaotong University.

The remaining parts of the paper are organized as follows. The definition of the proposed technique and the resultant TSO are introduced in Section 2. The mathematical criteria for quantitatively assessing the running condition of rotating machines are depicted in Section 3. The illustrative examples and the statistic results of the mathematical criteria for validating the proposed approach are presented in Section 4. Finally, the concluding remarks are given in Section 5.

2. Purifying shaft vibration signals using EMD

2.1. Definition

To facilitate understanding of the proposed technique, a couple of practical vibration signals collected using two perpendicularly mounted displacement transducers are used to illustrate step by step the procedures of the proposed method. These signals were from a rotating machine with a faulty coupling alignment. The time waveforms of the signals, their FFT spectra, and the shaft orbit constructed from them are shown in Fig. 1. The purified shaft orbit, derived using the HRS [1] are also given for comparison. It should be noted that $X(t)$ represents the signal collected in the x-direction and $Y(t)$ the y-direction.

According to the definition of the EMD [15,16], the signal to be investigated is decomposed into a finite number of IMFs, each of which represents a simple oscillatory mode and satisfies the following two conditions:

- In the whole data set of the IMF, the number of extrema and the number of zero crossings must either be equal or differ at most by one.
- At any point of the IMF, the mean value of the envelopes defined by the local maxima and minima is zero.

The first condition ensures the narrow band feature of the orthogonal filters implicit in the process of the EMD. The second condition ensures that the instantaneous frequency will not have any unwanted fluctuations induced by asymmetric waveforms. In the implementation of the EMD, a sifting process is conducted.

Step 1: Identify all local maxima in the signal $x(t)$ and then connect them by using a cubic spline line, which is regarded as the upper envelope and expressed by $e_u(t)$. Likewise, identify all local minima in $x(t)$ and connect them by using another cubic spline line, which is regarded as the lower envelope and expressed by $e_l(t)$.

Step 2: The local mean $m_1(t)$ is calculated by using the equation

$$m_1(t) = \frac{e_u(t) + e_l(t)}{2} \tag{1}$$

Step 3: Calculate the equation

$$h_1(t) = x(t) - m_1(t) \tag{2}$$

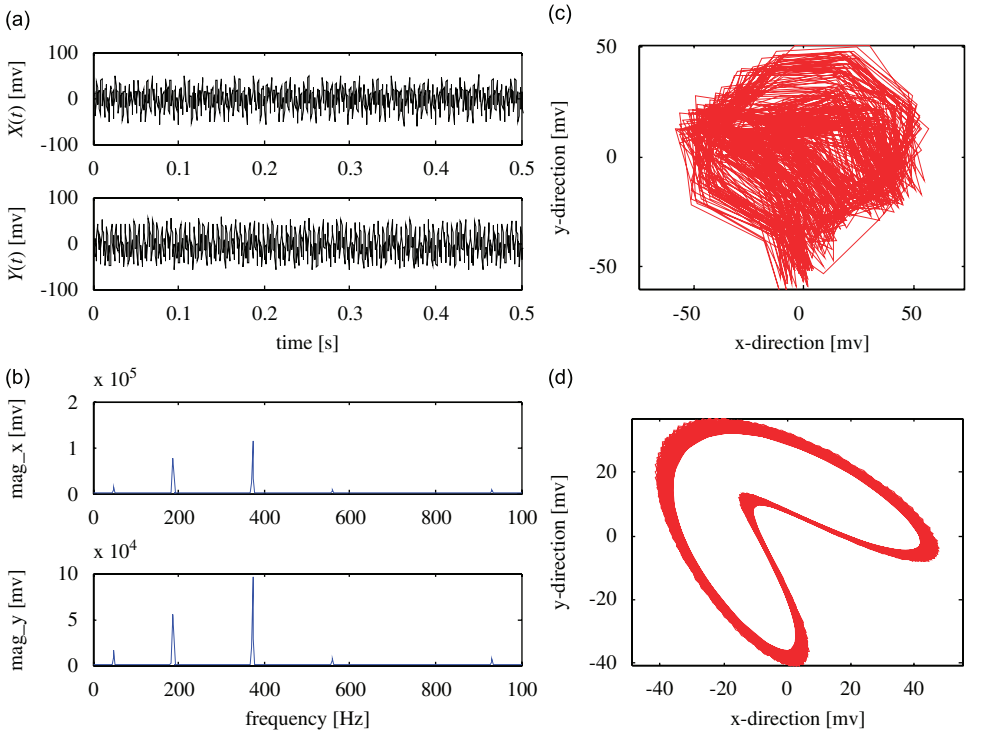

Fig. 1. The displacement signals when coupling misalignment fault happens in large rotating machinery: (a) time-waveforms of the signals, (b) FFT spectra of the signals, (c) original shaft orbit, and (d) purified shaft orbit derived by using the HRS.

and examine whether the resultant $h_1(t)$ is an IMF satisfying the aforementioned two conditions. If $h_1(t)$ is not an IMF, regard $h_1(t)$ as original signal and repeat above calculations until $h_1(t)$ is an IMF. Otherwise,

Step 4: Remove the first IMF from $x(t)$ and then get the residual component $r_1(t)$, i.e.

$$r_1(t) = x(t) - h_1(t) \tag{3}$$

Step 5: Treat $r_1(t)$ as original data and repeat above calculations until the second IMF $h_2(t)$ is obtained. Then

$$r_2(t) = r_1(t) - h_2(t) \tag{4}$$

Step 6: Iterate the previous calculations n times and get n IMFs of the signal until the final residual component:

$$r_n(t) = r_{n-1}(t) - h_n(t) \tag{5}$$

is a monotonic function or a constant from which no more IMF can be extracted.

Finally, the original signal $x(t)$ may be expressed as

$$x(t) = \sum_{i=1}^{n} h_i(t) + r_n(t) \tag{6}$$

By using this technique, the displacement signals $X(t)$ and $Y(t)$ shown in Fig. 1 are decomposed and the results shown in Fig. 2 are obtained. The FFT spectra of the obtained IMFs are also plotted in Fig. 2 to facilitate the interpretation of the EMD decomposition results.

Due to the narrow band feature of the 'orthogonal filters' implicit in the EMD process, each IMF should ideally contain only a single frequency component. However, in reality there is no perfect orthogonal filter, some interference terms are often present in the side bands of the principal IMF frequency. But these side band energies are small and the IMF is dominated by the principal frequency. Therefore, the distribution of signal

energy may be evaluated approximately through the ratio:

$$r_i = \sqrt{A_i} \Big/ \sum_{i=1}^{k} \sqrt{A_i} \quad (i = 1, 2, \ldots, k) \tag{7}$$

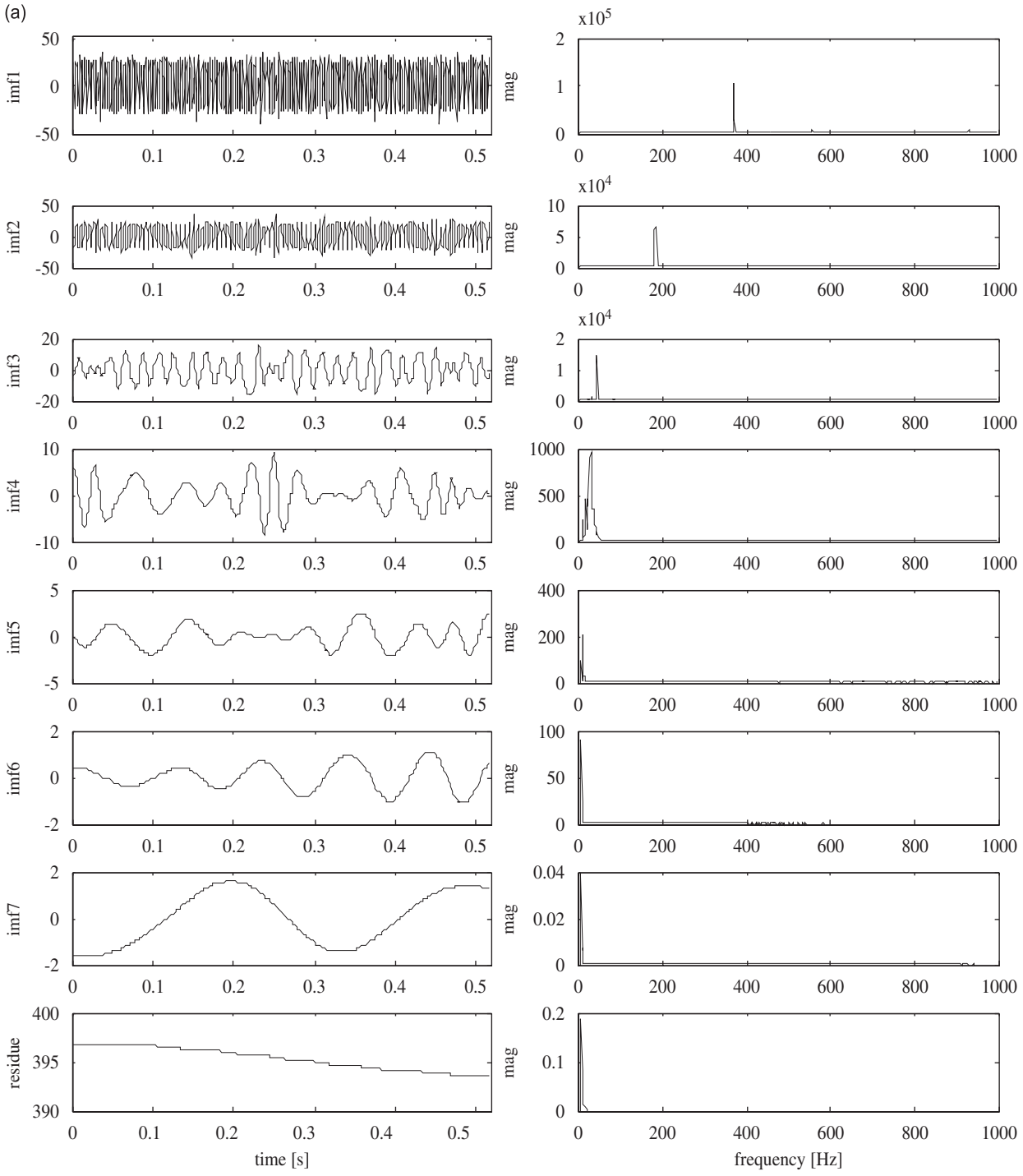

Fig. 2. The EMD of the displacement signals: (a) the EMD of signal $X(t)$ and (b) the EMD of signal $Y(t)$.

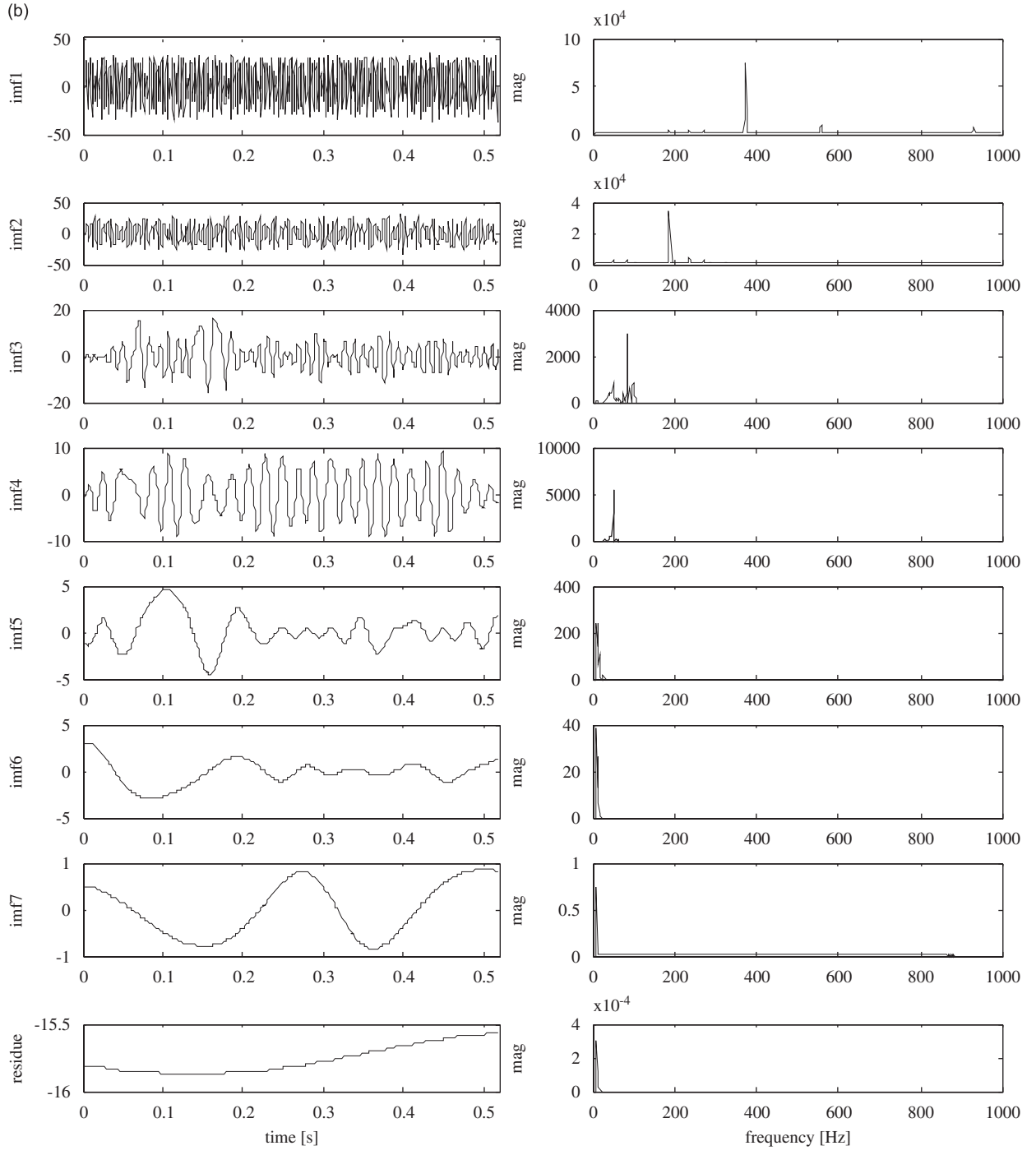

Fig. 2. (*Continued*)

where k indicates the number of the IMFs and A_i is the magnitude of the dominant frequency component in the i-th IMF. Likewise, the comprehensive energy distribution after considering the vibrations in both mutually orthogonal directions may be calculated by

$$r_{i\_xy} = \sqrt{r_{i\_x}^2 + r_{i\_y}^2} \Big/ \sum_{i=1}^{k} \sqrt{r_{i\_x}^2 + r_{i\_y}^2} \quad (i = 1, 2, \ldots, k) \tag{8}$$

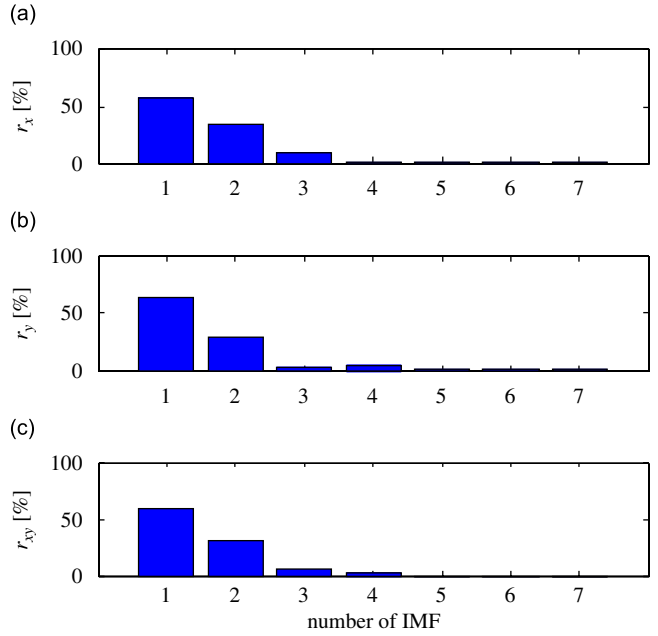

Fig. 3. Energy distributions of the signals $X(t)$ and $Y(t)$: (a) r_x, (b) r_y, and (c) r_{xy}.

where r_{i_x} and r_{i_y} represent the energy distribution ratios of the signals collected in x- and y-directions, respectively.

By using Eqs. (7) and (8), the energy distributions of the signals $X(t)$ and $Y(t)$ are calculated and the results are shown in Fig. 3.

Subsequently, sort r_{i_xy} $(i = 1, 2, \ldots, k)$ in descending order and identify the principal IMFs through the condition $\sum_{i=1}^{N} r_{i\_xy} \geqslant \theta_r$, where θ_r is a threshold with default value 0.8. In practical calculations, θ_r may have any value in the interval (0, 1). The larger θ_r, the greater the number of IMFs that need to be taken into account for constructing the 'purified' signal. In this paper, the default value of 0.8 is adopted. Based on this rule, the first and the second IMFs in Fig. 3 are identified as the principal IMFs of the signals. Long-term large rotating machine fault diagnosis shows that twice shaft-rotational frequency is a typical symptom of coupling misalignment. By observing Fig. 2, it is found that the dominant frequency of the second IMF is the shaft-rotational frequency 190 Hz, the dominant frequency of the first IMF is the twice shaft-rotational frequency 380 Hz. So, there is no doubt that the EMD has successfully extracted the major features of the shaft vibration.

In order to further remove interference terms from the principal IMFs, an adaptive band-pass filter $f(t)$ is designed, inspired by the thought of Morlet wavelet function [13], $f(t)$ may be mathematically expressed as

$$f(t) = \mathrm{e}^{-(2t/\xi)^2/2} \sin(\omega t + \varphi) \quad \left(t = 0 \sim \frac{L-1}{f_s}, \varphi = 0 \right) \tag{9}$$

whose central frequency ω is adaptively the dominant frequency of the IMF being considered. In the equation, ξ is a shape-control parameter of a Gaussian window, f_s is the sampling frequency of the original vibration signal, and L is the number of data used to simulate the filter. Together with parameter ξ, it determines the time–frequency resolution and the bandwidth of the filter.

An illustrative example is given in Fig. 4, showing the influences of ξ and L on the filter bandwidth. From Fig. 4, it is found that the larger the values of ξ and L, the narrower the bandwidth of the filter.

In this paper, an adaptive L is used in order to achieve high frequency resolution at low frequencies and high time resolution at high frequencies. It is calculated by using the equation

$$L = \frac{f_s}{2f_{\mathrm{imf}}} L_0 \tag{10a}$$

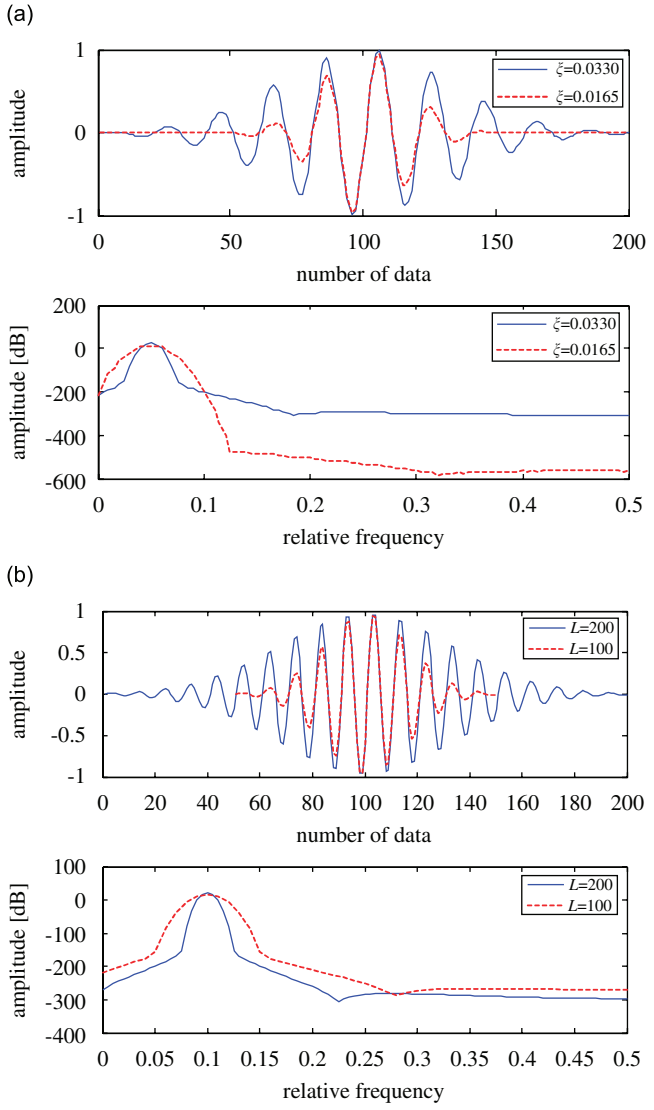

Fig. 4. Influences of ξ and L on the bandwidth of the filter: (a) influence of ξ and (b) influence of L.

where f_{imf} indicates the dominant IMF frequency being considered, L_0 is the number of data used for simulating the filter when the dominant frequency of the IMF is as high as half the sampling frequency of the signal. In this paper, $L_0 = 100$. The value of the shape-control parameter ξ is dependant upon the value of L, i.e.

$$\xi = \frac{L}{f_s\sqrt{2\log 100}} \tag{10b}$$

Then, the principal IMFs are filtered using the equation:

$$\tilde{x}_{\mathrm{imf}\_i}(t) = \int_{-\infty}^{+\infty} x_{\mathrm{imf}\_i}(\tau) f(t-\tau)\,\mathrm{d}\tau \tag{11}$$

where $x_{\mathrm{imf}\_i}(t)$ represents the i-th principal IMF and $\tilde{x}_{\mathrm{imf}\_i}(t)$ is its purified result.

In order to conserve energy $\tilde{x}_{\mathrm{imf}\_i}(t)$ is further normalized by the equation

$$\tilde{\tilde{x}}_{\mathrm{imf}\_i}(t) = \tilde{x}_{\mathrm{imf}\_i}(t)\sqrt{\frac{A_i}{\tilde{A}_i}} \tag{12}$$

where A_i is the magnitude of the dominant frequency component in the i-th principal IMF. $\tilde{A}_i$ is the magnitude of the dominant frequency component in $\tilde{x}_{\mathrm{imf}\_i}(t)$.

Finally, the 'purified' signal is constructed using the equation

$$X_p(t) = \sum_{i=1}^{N} \tilde{\tilde{x}}_{\mathrm{imf}\_i}(t) \tag{13}$$

where N indicates the number of principal IMFs and $X_p(t)$ represents the 'purified' signal constructed using them.

After processing both $X(t)$ and $Y(t)$ using the method described above, their 'purified' forms $X_p(t)$ and $Y_p(t)$ as well as the 'purified' shaft orbit constructed from them are shown in Fig. 5a, where the typical 'banana' or '8' shaped shaft orbit of a coupling misalignment fault is clearly observed, while this symptom cannot be observed directly from the original shaft orbit in Fig. 1c. Unlike the HRS, the EMD does not require any complex calculations for obtaining the accurate amplitude, frequency, and phase information from the signals.

In order to show the superiority of the EMD-based approach, the original shaft orbit, shown in Fig. 1c, is also purified using the method of wavelet packet decomposition adopted in Refs. [2–4]. The purified results are also shown in Fig. 5 for the convenience of comparison. In the wavelet packet decompositions, an orthogonal wavelet function namely 'haar' wavelet was used. In Fig. 5b and c, '$W_{m,n}$' ($n \geqslant 0$) indicate the coefficients located in the no. $n+1$ frequency region obtained during the m-level of wavelet packet decomposition. Herein, $m = 3$ implies that the three-level of wavelet packet decomposition was conducted to interpret the shaft vibratory signals $X(t)$ and $Y(t)$. The purified signals (x_{wp} and y_{wp}) are constructed using the coefficients $W_{3,1}$, $W_{3,2}$ and $W_{3,3}$, in which the frequencies characterizing the coupling misalignment fault are contained.

From Fig. 5b and c it is found that many interference terms exist in each $W_{m,n,}$, as a consequence, the purified shaft orbit shown in Fig. 5d is noisy and the characteristic 'banana' or '8' shape cannot be identified.

In the meantime, the computing efficiency of the EMD-based approach is verified by comparison with the three-level of wavelet packet decomposition algorithm. In the investigation, the computer program for each approach was run 10 times. The recorded computing times and their mean values are listed in Table 1. This investigation was carried out on a common computer with a 3.40 GHz Pentium(R) D CPU and a 1 GB RAM.

From Table 1, it is obvious that the EMD-based approach is more time-efficient than the three-level of wavelet packet decomposition-based approach as the former takes an average of 1.5141 s to get the 'purified' orbit shown in Fig. 5a, while the latter takes average 2.0828 s to get the purified orbit shown in Fig. 5d. When a higher-level of wavelet packet decomposition is employed, the computing time-efficiency will be lower.

2.2. Transient shaft orbit (TSO)

Practice shows that the two-dimensional shaft orbit cannot always provide adequate shaft vibration information, thus an incorrect diagnosis may be inevitable. The EMD approach provides an effective way to improve this situation, attributable to the IMFs giving a real description of the signal with time. To facilitate understanding of this statement, Fig. 6 shows a two-dimensional shaft orbit obtained during start-up of a centrifugal compressor.

By observing the orbit shown in Fig. 6 it is hard to explain why the shaft orbit appears to show two orbit tracks. It has even been wrongly concluded that chaos or an oil whirl fault is occurring because the orbit has features similar to them. However, this can easily be clarified using the EMD method. In this way a new concept is proposed, the TSO, taking the advantages of the IMFs, which provide a real time description of the signal. In essence, the TSO is a three-dimensional shaft orbit constructed by introducing time into the conventional two-dimensional shaft orbit. The TSO corresponding to the orbit in Fig. 6 is shown in Fig. 7.

With the aid of the TSO in Fig. 7, it can easily be understood that the two tracks of the orbit are formed at different times, i.e. before and after the shaft passes through its first-order critical speed. The TSO gives more

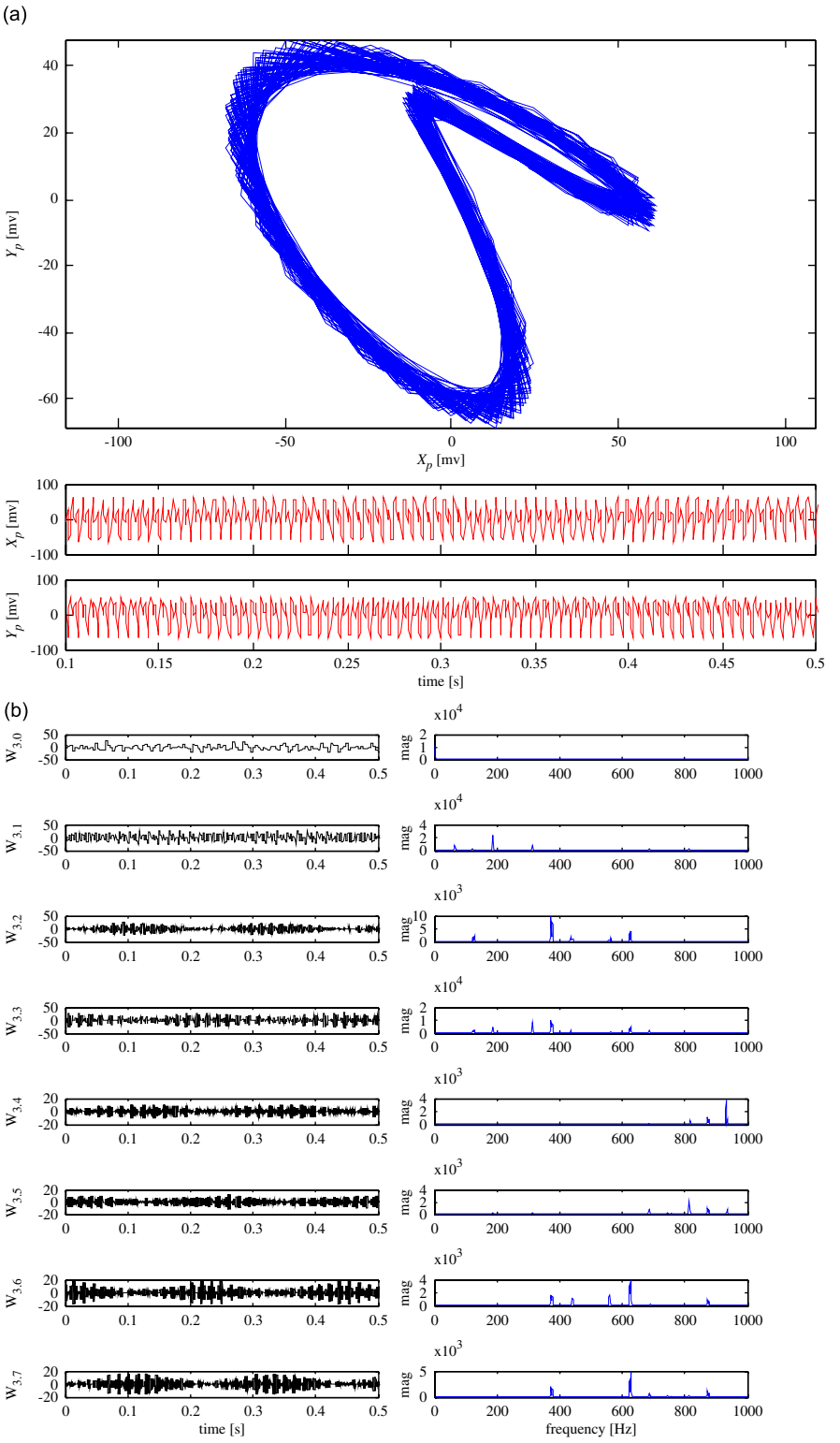

Fig. 5. Signals and purified orbit: (a) 'purified' vibration signals and 'purified' shaft orbit derived by the EMD, (b) three-level wavelet packet analysis of $X(t)$, (c) three-level wavelet packet analysis of $Y(t)$, and (d) purified signals and purified orbit derived by using the wavelet packet decomposition coefficient x_{wp} and y_{wp}, both of them are constructed by $W_{3,1}+W_{3,2}+W_{3,3}$.

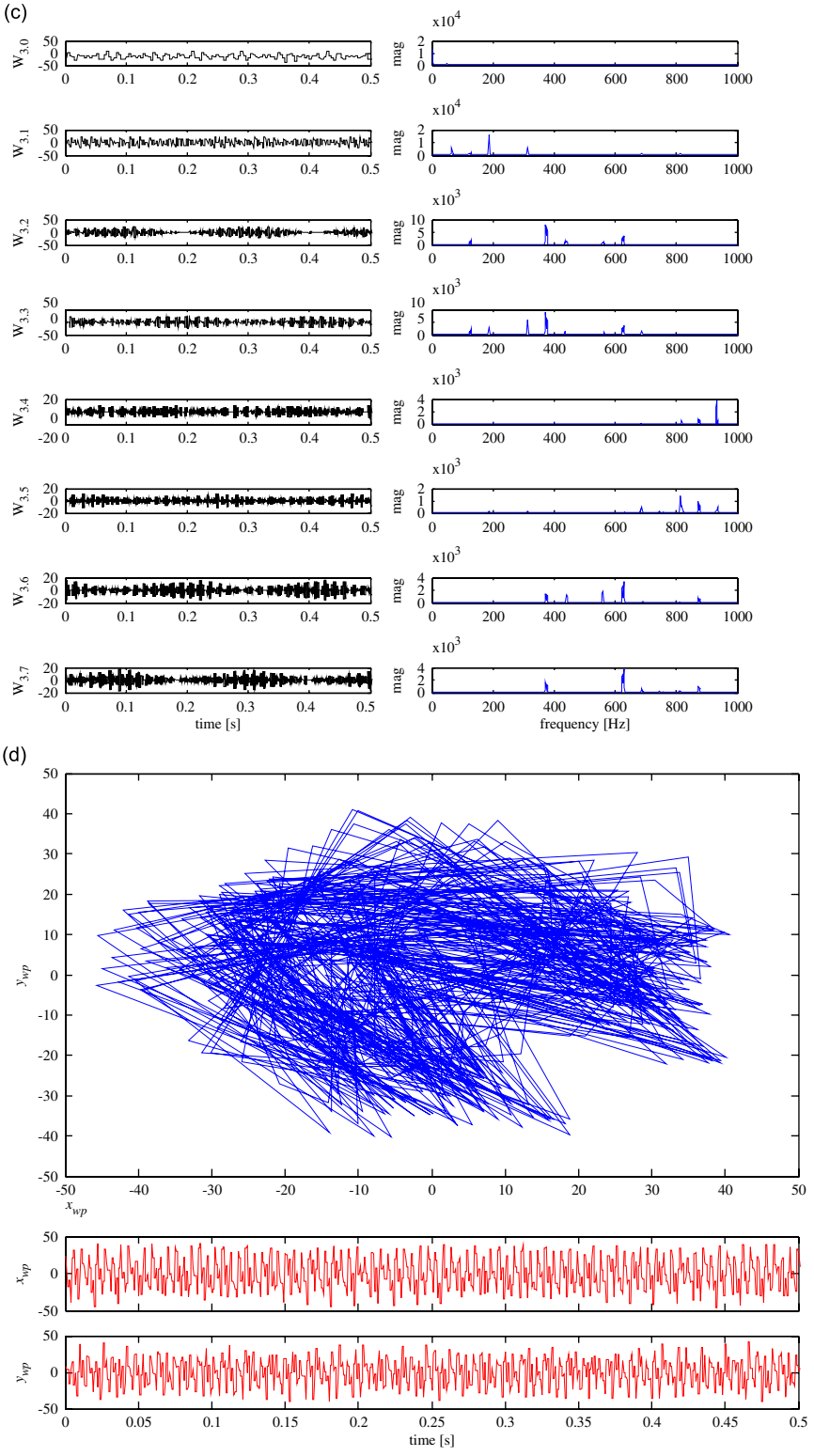

Fig. 5. (*Continued*)

Table 1
Computing efficiency of the EMD approach.

Computer run no.	Computing time for getting the purified shaft orbits shown in Fig. 5 (s)	
	EMD-based approach	Wavelet packet decomposition-based approach
1	1.5313	2.1560
2	1.5156	2.0469
3	1.5313	2.0781
4	1.4844	2.1094
5	1.5625	2.0781
6	1.5313	2.0781
7	1.4531	2.0781
8	1.5156	2.0625
9	1.4844	2.0938
10	1.5313	2.0469
Mean (s)	1.5141	2.0828

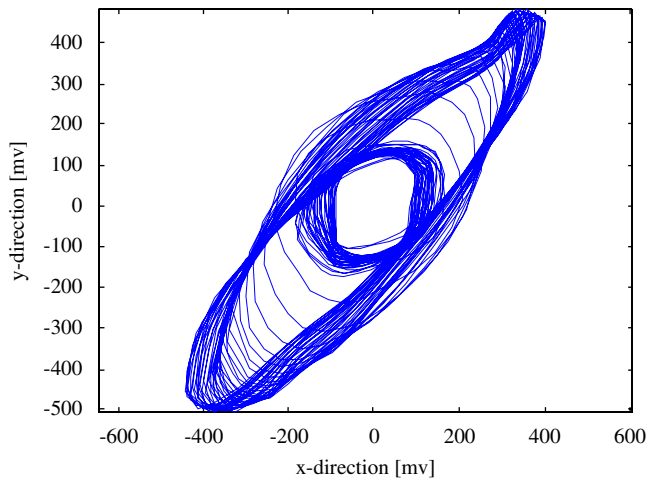

Fig. 6. A two-dimensional shaft orbit obtained during start-up period.

machine condition monitoring and fault diagnosis information than conventional two-dimensional shaft orbits.

However, the true TSO cannot be obtained using the FT.

The WT is a potential method, but it is not efficient due to the complex calculations involved in WTs and inverse WTs. In contrast, the EMD-based approach provides an ideal way to construct the TSO, whatever in computational accuracy or algorithmic efficiency.

3. Mathematical criteria for assessing the IMFs and the TSO

Nine mathematical criteria, R_l, R_o, R_u, F, s_1–s_5, are now proposed for describing the vibration information exhibited by the IMFs and the TSO, so that the running condition of a machine may be quantitatively assessed.

Different faults show different energy distributions in the frequency domain and the EMD decomposes the signal into a series of IMFs in descending order of frequency. The following three criteria are proposed to

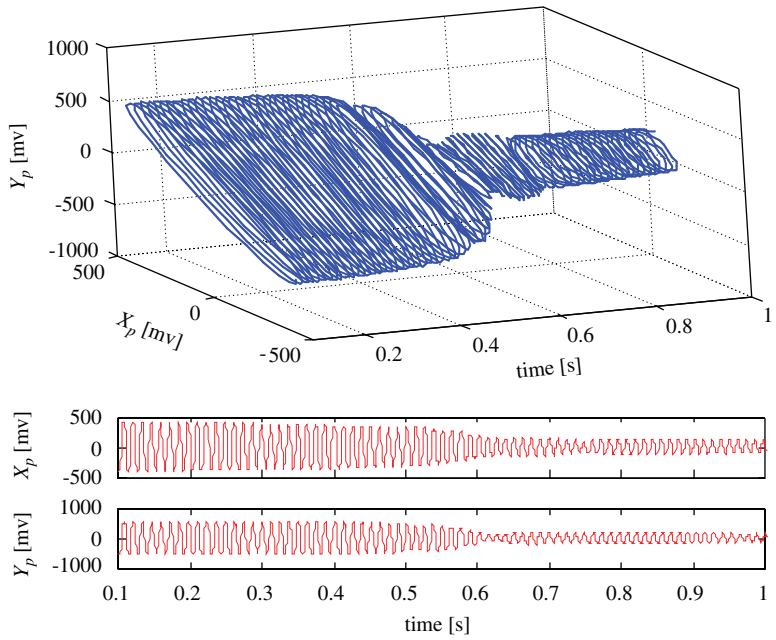

Fig. 7. The TSO corresponding to the shaft orbit shown in Fig. 6.

detect changes of shaft vibration energy distribution. Assume $\tilde{\tilde{A}}_{i\_x}$ and $\tilde{\tilde{A}}_{i\_y}$ ($i = 1,2,\ldots,N$) are the magnitudes of the dominant frequency components in $\tilde{\tilde{x}}_{\mathrm{imf}\_i}(t)$ and $\tilde{\tilde{y}}_{\mathrm{imf}\_i}(t)$, which are the 'purified' principal IMFs, respectively, in the x- and y-directions.

$\tilde{\tilde{A}}_{k\_x}$ and $\tilde{\tilde{A}}_{k\_y}$ ($k = 1,2,\ldots,0 \leqslant K \leqslant N$) are the magnitudes of those 'purified' principal IMFs whose dominant frequencies f_{imf_k} are smaller than the shaft rotational frequency f_r, i.e. $f_{\mathrm{imf}\_k} < f_r$. $\tilde{\tilde{A}}_{o\_x}$ and $\tilde{\tilde{A}}_{o\_y}$ are the magnitudes of the 'purified' principal IMFs whose dominant frequencies are equal to f_r. Then, the energy distribution of the shaft vibration may be described by the following three criteria R_l, R_o, R_u:

$$R_l = \frac{\sum_{k=1}^{K} \sqrt{\tilde{\tilde{A}}_{k\_x} + \tilde{\tilde{A}}_{k\_y}}}{\sum_{i=1}^{N} \sqrt{\tilde{\tilde{A}}_{i\_x} + \tilde{\tilde{A}}_{i\_y}}} \tag{14}$$

$$R_o = \frac{\sqrt{\tilde{\tilde{A}}_{o\_x} + \tilde{\tilde{A}}_{o\_y}}}{\sum_{i=1}^{N} \sqrt{\tilde{\tilde{A}}_{i\_x} + \tilde{\tilde{A}}_{i\_y}}} \tag{15}$$

$$R_u = 1 - R_l - R_o \tag{16}$$

Among which, R_l indicates the proportion of the energy contributed by low-frequency vibrations, R_o the proportion contributed by shaft rotational frequency component, and criterion R_u is the proportion contributed by high-frequency vibrations.

In order to measure the singularity of the TSO, the curvature of the orbit is calculated by using the equation

$$\zeta(t) = \frac{\dot{X}_p(t)\ddot{Y}_p(t) - \ddot{X}_p(t)\dot{Y}_p(t)}{\{[\dot{X}_p(t)]^2 + [\dot{Y}_p(t)]^2\}^{3/2}} \tag{17}$$

where $X_p(t)$ and $Y_p(t)$ represent the 'purified' vibration signals, respectively, in the x- and y-directions. As in Ref. [1] the maximum value of $\zeta(t)$ is employed to evaluate the smoothness of the shaft orbit, i.e.

$$F = \max(|\zeta(t)|) \tag{18}$$

Experimental results reveal that F approximates to 1 when the shaft runs normally. Its value diverges from 1 in the presence of a mechanical fault. Moreover, the bigger the divergence, the more serious the indicated fault.

For various dynamic reasons, the shaft orbit often shows different geometric shapes at different times. Transient changes of the TSO often include vital information for machine diagnosis. For example, sudden changes of the orbit shape and position can be observed when rotor-to-stator rubbing occurs; the swaying motion of the shaft indicates the presence of a part-loosening fault; a fluid excitation fault usually leads to irregular changes of shaft vibration intensity and orientation, but without changing the central position of the shaft.

In order to extract these characteristics from the TSO, the following five criteria, s_1–s_5, are proposed. For facilitating the understanding, a schematic diagram is plotted in Fig. 8, in which a single cycle of transient shaft vibration orbit is shown and

$$r_j(i-jM+M)=\sqrt{[X_p(i)]^2+[Y_p(i)]^2} \tag{19}$$

where $i=\{(j-1)M+1,(j-1)M+2,\ldots,jM\}$, $M=f_s/f_r$ which indicates the number of data collected in a single shaft rotating cycle, $j=\{1,2,\ldots,D\}$, D represents the number of shaft rotating cycles contained in the whole signal.

In Fig. 8,

$$a=\max(r_j(i-jM+M)) \tag{20}$$

$$b=\min(r_j(i-jM+M)) \tag{21}$$

Let

$$\ell(j)=\frac{a}{b} \tag{22}$$

Then, have

$$s_1=\frac{1}{D}\sum_{j=1}^{D}[\ell(j)-\bar{\ell}(j)]^2 \tag{23}$$

where $\bar{\ell}$ is the mean value of ℓ.

The criterion s_1 indicates the stability of shaft vibration. The smaller the value of s_1, the more stable the shaft vibration.

In order to measure the symmetric property of the shaft vibration in different circumferential directions, r_j is employed directly to construct another criterion s_2, i.e.

$$s_2=\frac{1}{D}\sum_{j=1}^{D}\hbar_j \tag{24}$$

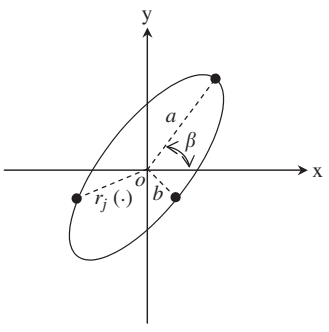

Fig. 8. Single cycle of transient shaft vibration orbit.

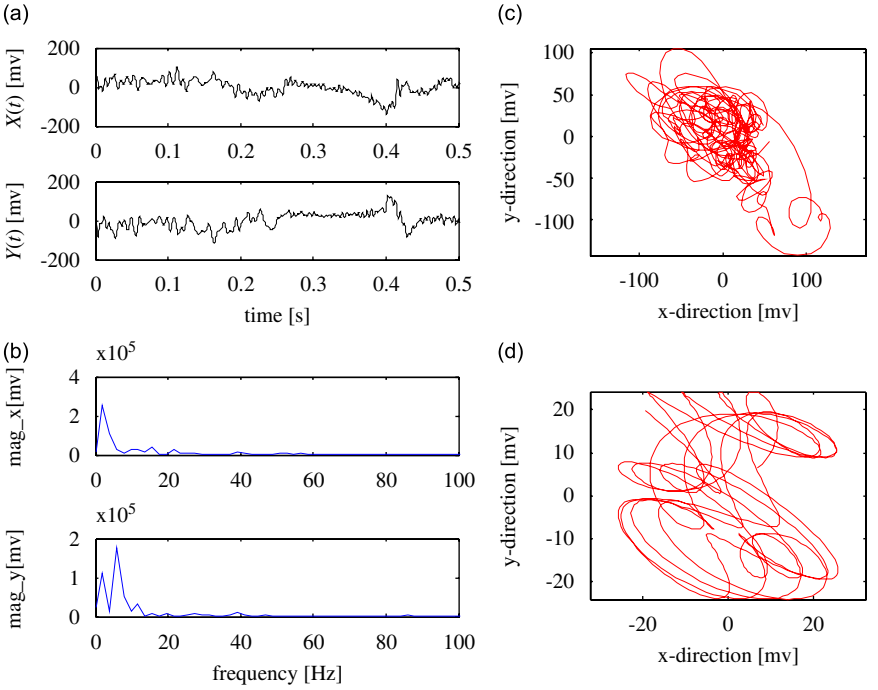

Fig. 9. Part-loosening faulty signals: (a) time-waveforms of the signals, (b) FFT spectra of the signals, (c) original shaft orbit, and (d) purified shaft orbit derived by the HRS.

where

$$\hbar_j = \frac{1}{M}\sum_{n=1}^{M}[\vartheta_j(n) - \bar{\vartheta}_j(n)]^2 \tag{25}$$

and

$$\vartheta_j(n) = \frac{r_j(n)}{\max(r_j)} \tag{26}$$

It is well known that the inclination angle of the major axis of the orbit reflects the relative magnitudes of the mechanical forces on the shaft. A change in this angle often indicates a change in machine running conditions, for example, the presence of rotor-to-stator rubbing will lead to a frequent change of this angle. However, this does not happen in the presence of a fluid pipe excitation fault, in which case the inclination angle shows an invariant value. Anyway, the variation of this angle may be described by the criterion s_3:

$$s_3 = \frac{1}{D}\sum_{j=1}^{D}[\beta(j) - \bar{\beta}(j)]^2 \tag{27}$$

where $\beta(j) = \text{a tan}(Y_p(m)/X_p(m))$, $X_p(m)$, and $Y_p(m)$ are the amplitudes of the 'purified' signals when $r_j(i)$ reaches its maximum value in the j-th shaft rotating cycle.

Practice shows that both very large and very small values of s_3 indicate the presence of machine faults.

The residual of the EMD reveals the trend of the signal being investigated and in the present application represents variations of the central position of the shaft, which may be expressed as

$$P_{\text{center}}(t) = \rho(t)\,\vec{\theta}(t) \tag{28}$$

where

$$\rho(t) = \sqrt{[x_{\text{residue}}(t)]^2 + [y_{\text{residue}}(t)]^2} \tag{29}$$

$$\theta(t) = \text{a tan}\left(\frac{y_{\text{residue}}(t)}{x_{\text{residue}}(t)}\right) \tag{30}$$

$x_{\text{residue}}(t)$ and $y_{\text{residue}}(t)$ are the residues in the EMDs of $X(t)$ and $Y(t)$.

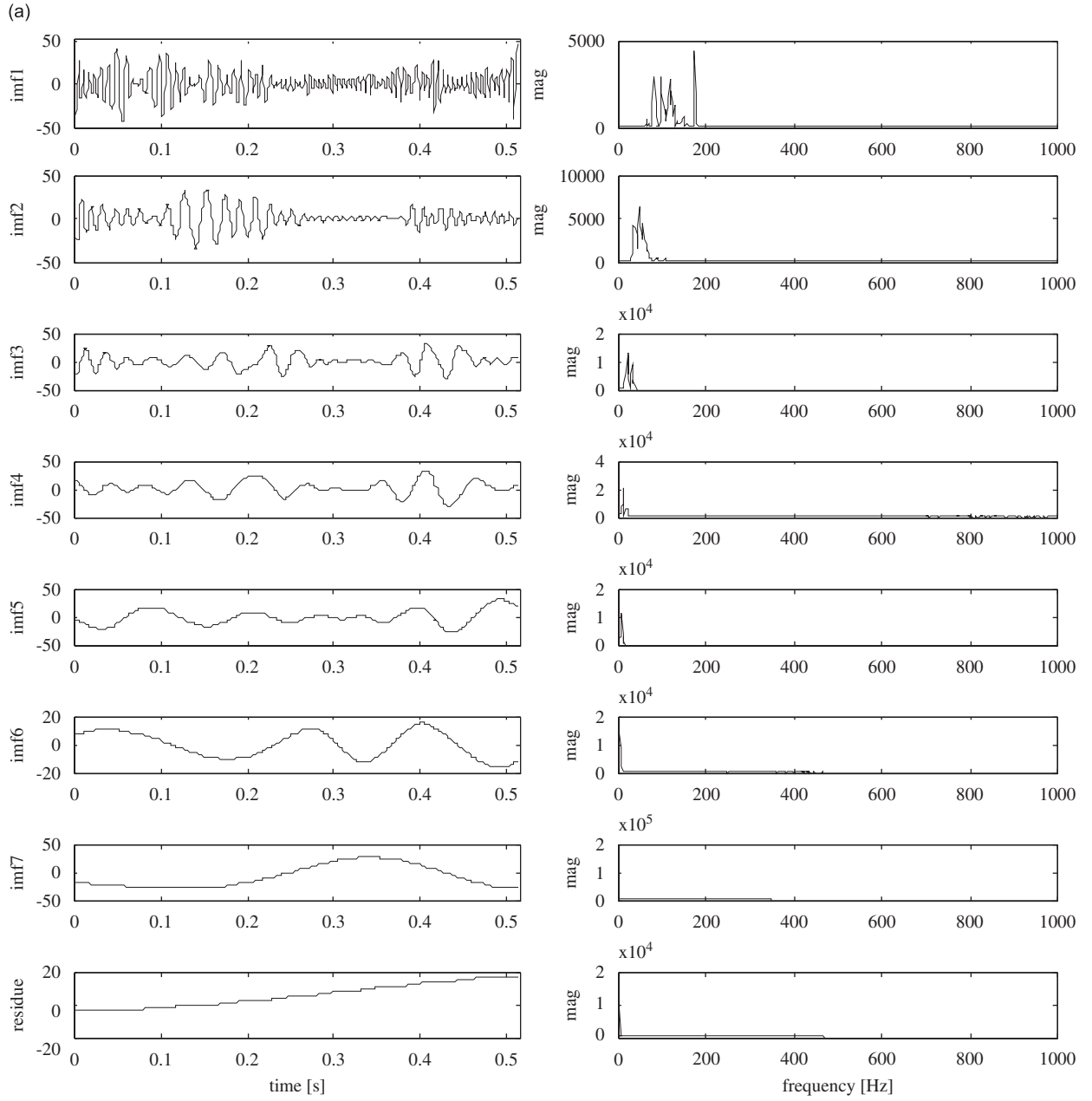

Fig. 10. The EMDs of the part-loosening faulty signals: (a) signal in x-direction, (b) signal in y-direction, and (c) energy-distribution figures.

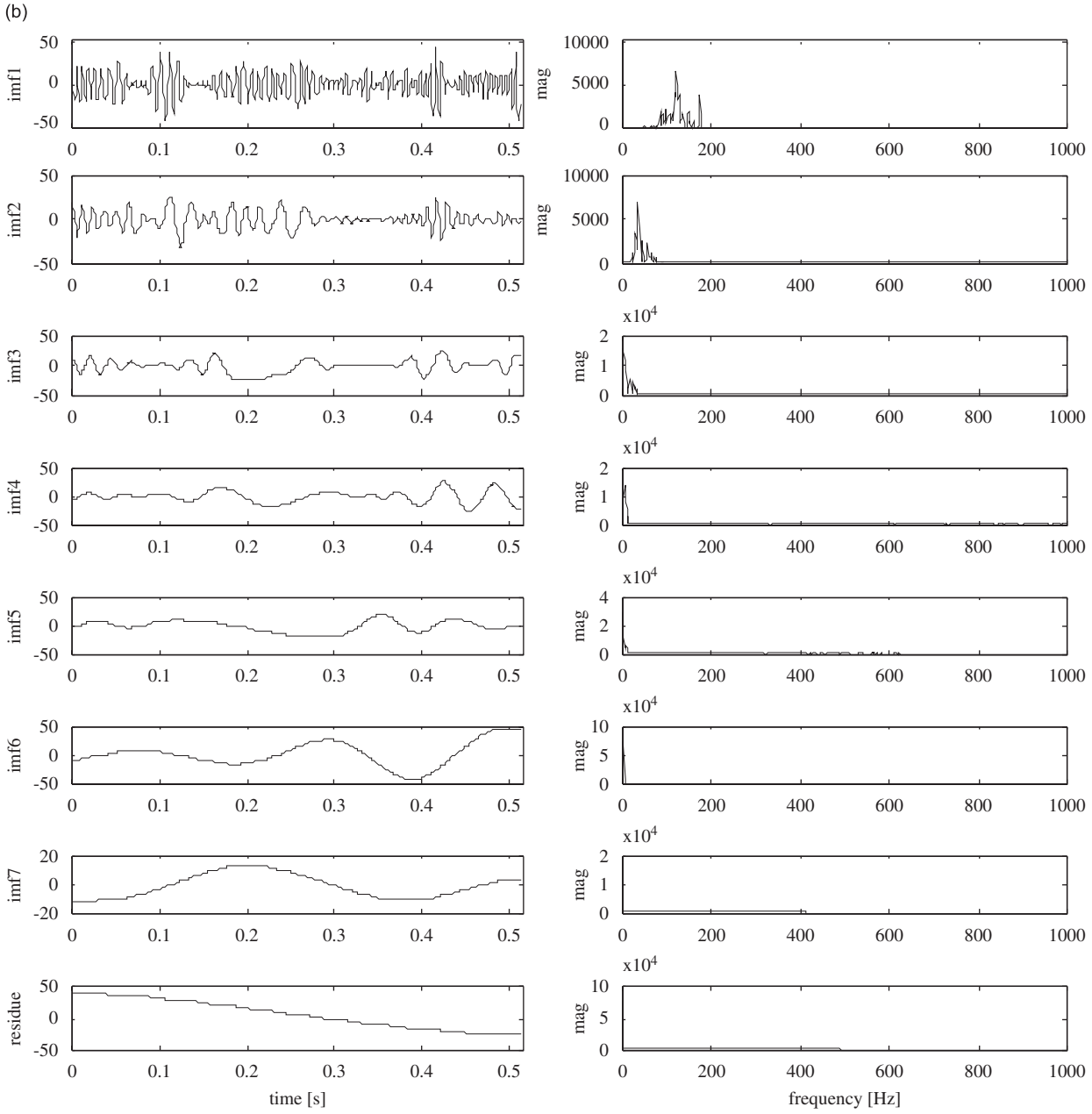

Fig. 10. (*Continued*)

Obviously, changes of $\rho(t)$ and $\theta(t)$ both indicate a change in the central position of the shaft. In order to measure movement of the shaft's central position with respect to the bearing housing, the following two criteria, s_4 and s_5 are proposed with the aid of $\rho(t)$ and $\theta(t)$, i.e.:

$$s_4 = \frac{1}{T}\sum_{t=0}^{T}[\rho(t) - \bar{\rho}(t)]^2 \tag{31}$$

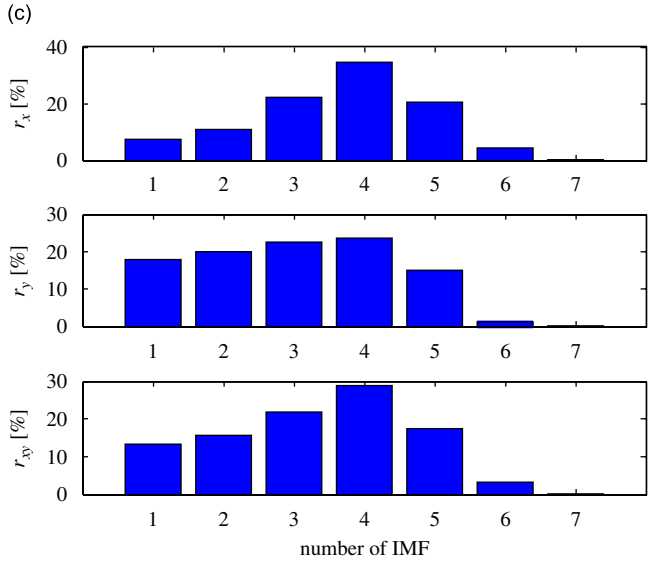

Fig. 10. (*Continued*)

$$s_5 = \frac{1}{T}\sum_{t=0}^{T}[\theta(t) - \bar{\theta}(t)]^2 \tag{32}$$

where T is the time duration of the signals being investigated.

4. Verification of the proposed technique

The effectiveness of the proposed technique in condition monitoring and fault diagnosis of rotating machines is validated in the following.

4.1. The EMD-based TSO in fault diagnosis

Firstly, a couple of part-loosening fault signals from centrifugal compressors are considered. Their time waveforms, FFT spectra, and the shaft orbit constructed by them are shown in Fig. 9, in which the purified shaft orbit obtained by the approach of the HRS is also given for comparison.

The signals in both x- and y-directions are analyzed by using the EMD and the resultant IMFs are shown in Fig. 10.

From Fig. 10a and b, it is observed that the EMD does provide a perfect decomposition of the signal in both time and frequency domains. The energy leakage phenomenon existing in the WTs (observed in Fig. 5b and c) has been significantly reduced in the IMFs. From Fig. 10c, it can be seen that the first five IMFs are the principal IMFs. Then, by processing the principal IMFs using the adaptive filter depicted in Section 2 and constructing the 'purified' signals using Eq. (13), the x- and y-'purified' signals and the TSO constructed from them are shown in Fig. 11, in which the original vibration signals and their TSO are plotted for comparison.

The comparison of Figs. 11a and 9 shows that the EMD-based 'purified' TSO provides a more realistic and natural description of the shaft vibration. In other words, the transient swaying of the shaft central position due to part loosening has been vividly exhibited by the TSO. However, this phenomenon cannot be observed so clearly from the purified orbit by the HRS. Undoubtedly, a reliable assessment of the machine condition may be achieved more easily with the aid of the TSO derived by the EMD.

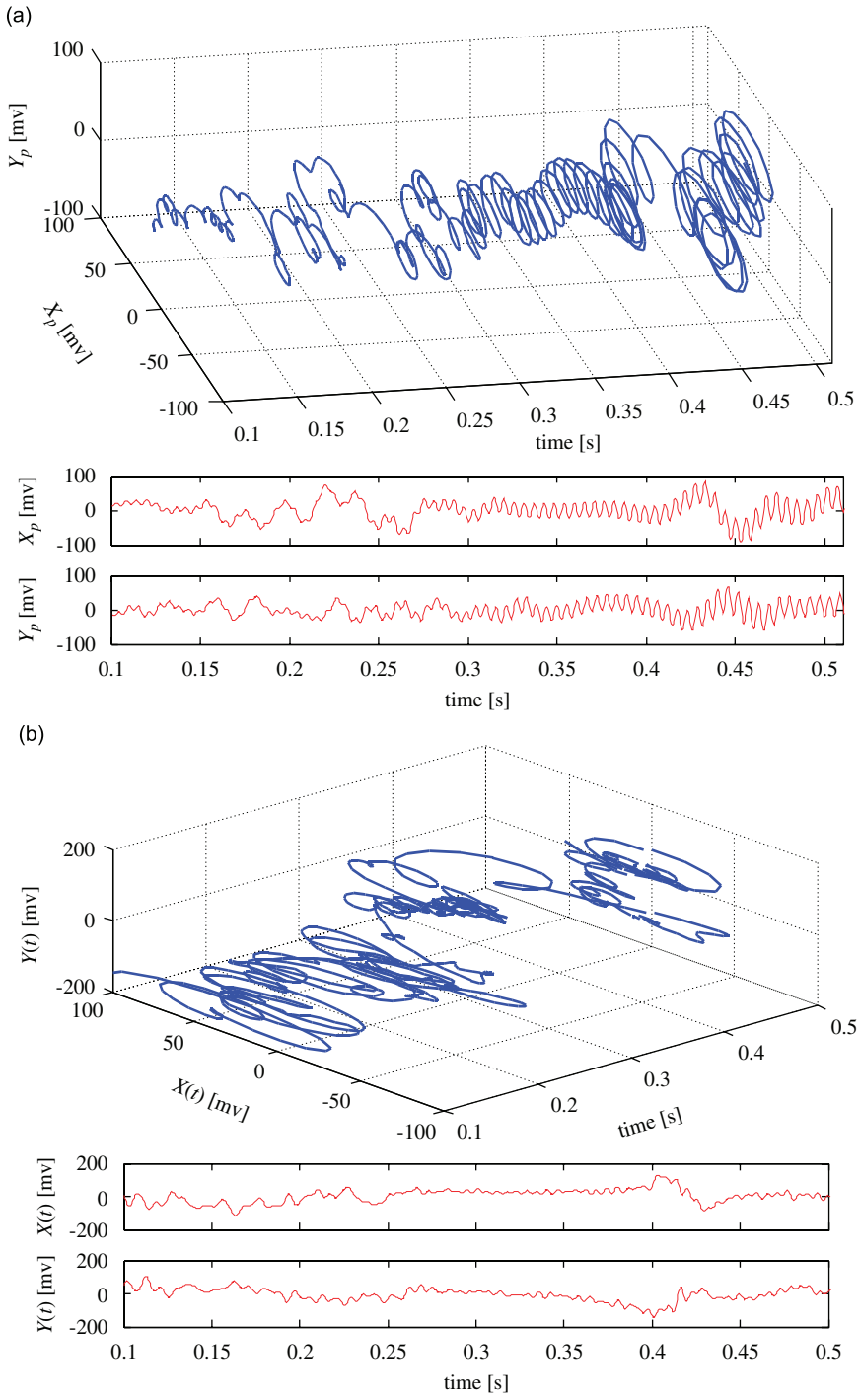

Fig. 11. The TSO in the presence of part-loosening fault: (a) TSO by the EMD-based approach and (b) TSO by the original shaft vibration signals.

In the meantime, the comparison of Fig. 11a and b suggest that the TSO derived using the EMD approach shows a clearer indication of machine running condition than the TSO constructed using the original shaft vibration signals. This is because vibrations unrelated to the fault have been removed from the former.

One more proof for validating the proposed approach is the diagnosis of a fluid excitation fault occurring in a centrifugal compressor. The time waveforms and FFT spectra of the original signals and the shaft orbits constructed from them are shown in Fig. 12.

Both the original and purified shaft orbit in Fig. 12 show unclear information and nothing can be concluded from them. The EMD approach is then applied to the signals and the derived IMFs and their energy distributions are shown in Fig. 13.

By observing the r_{xy} shown in Fig. 13c, it is found that the second, third, forth, and the fifth IMFs are the principal IMFs. Likewise, the adaptive filtering technique is applied to them to obtain their 'purified' forms. The 'purified' signals and the TSO constructed from them are shown in Fig. 14 together with the original shaft vibration signals and their corresponding TSO for comparison.

From Fig. 14a, it is observed that not only the orbit vibration intensity changes irregularly, but also the major-axis inclination, due to the random excitation from the fluid excitation. However, these phenomena cannot be observed clearly from Fig. 14b. It is also found that the central position of the shaft does not change in the presence of this fault. This is distinctly different from the TSO in the part-loosening fault, Fig. 11a, and the TSO in the rotor-to-stator rubbing fault, Fig. 15e. While, the TSO shown in Fig. 15e is different from that in Fig. 11a too. In other words, the sharp changes of the orbit observed in Fig. 15b are not present in the TSO when a part-loosening fault occurs, though the fluctuation of shaft central position occurs in both cases. Therefore machine faults with similar vibrations but different characteristics can easily be distinguished from each other with the aid of a TSO derived from the EMD.

4.2. The mathematical criteria

The mathematical criteria proposed in Section 3 are now calculated to verify their effectiveness in describing transient shaft vibrations under different machine running conditions. In these calculations, total seven different machine running conditions are considered. They are:

- coupling misalignment,
- part-loosening,

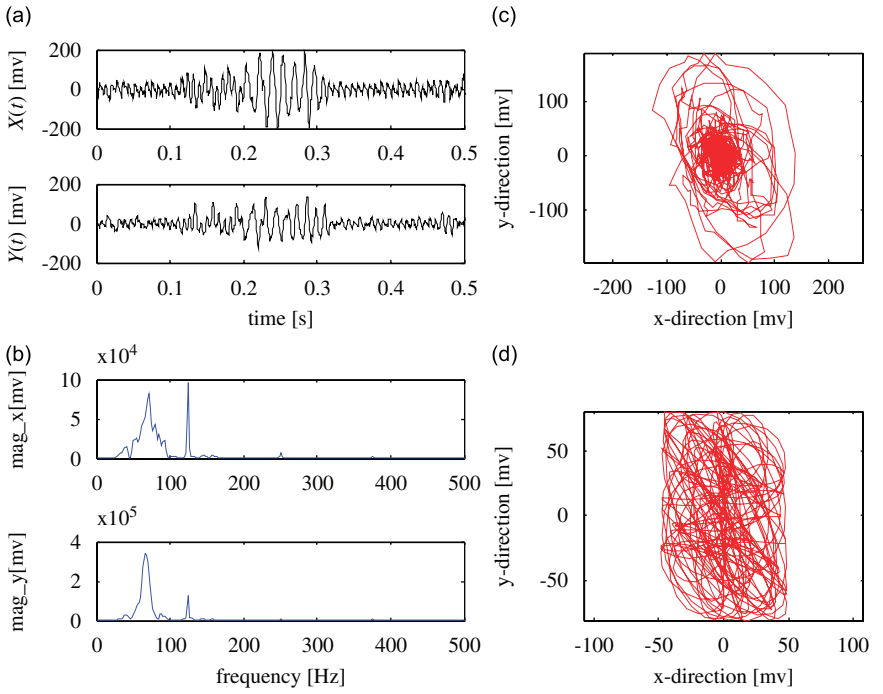

Fig. 12. Fluid excitation faulty signals: (a) time-waveforms of the signals, (b) FFT spectra of the signals, (c) original shaft orbit, and (d) purified shaft orbit derived by using the HRS.

- rotor-to-stator rubbing,
- fluid excitation,
- oil whirl,
- incipient transverse cracking, and
- normal running condition of the shaft.

Each condition is investigated by calculating the criteria from 12 pairs of sample signals collected from real centrifugal compressors, with similar rotor-bearing systems, operating in the Shijiazhuang Petroleum Plant,

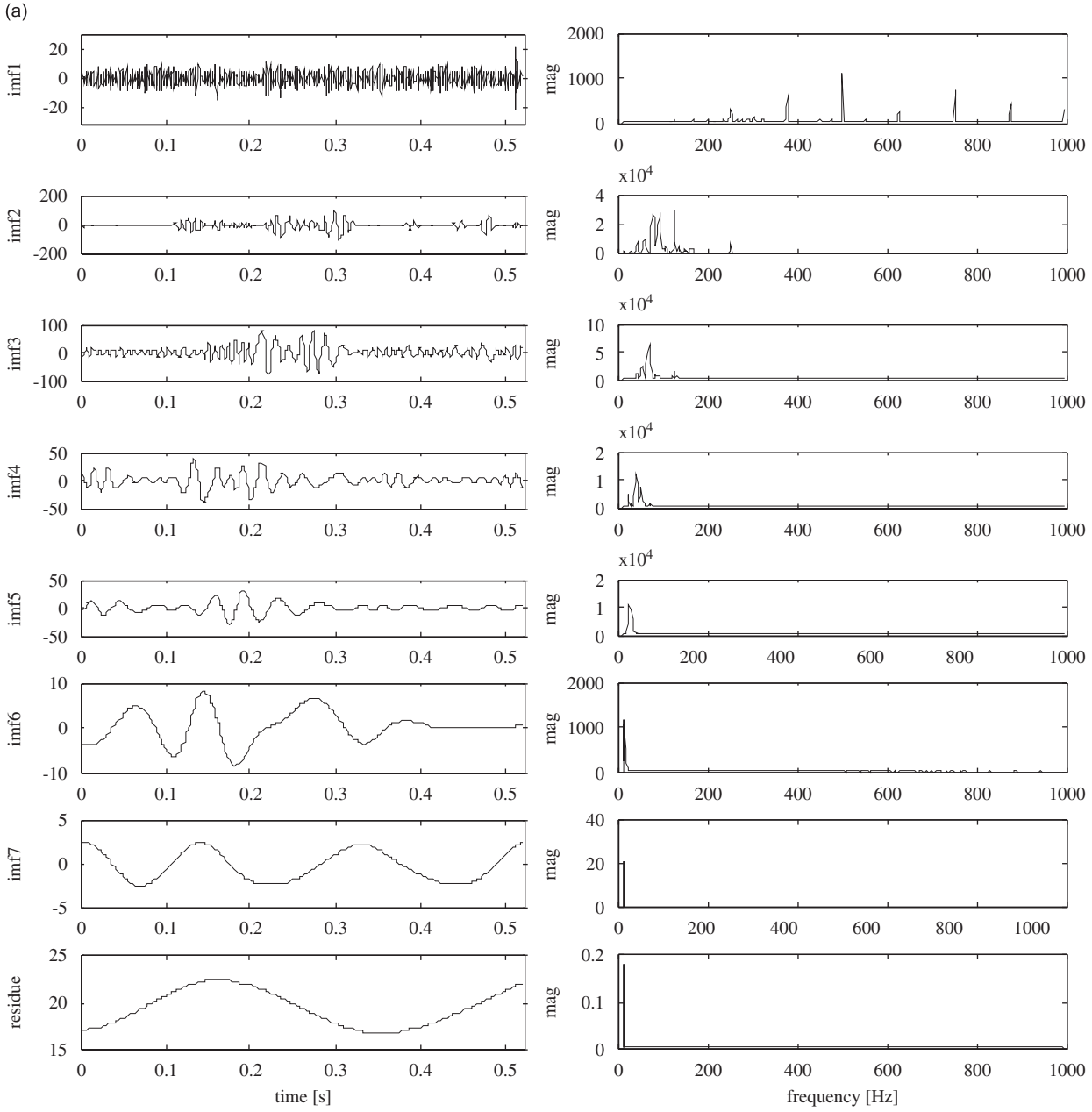

Fig. 13. The EMDs of the fluid excitation faulty signals: (a) signal in x-direction, (b) signal in y-direction, and (c) energy-distribution figures.

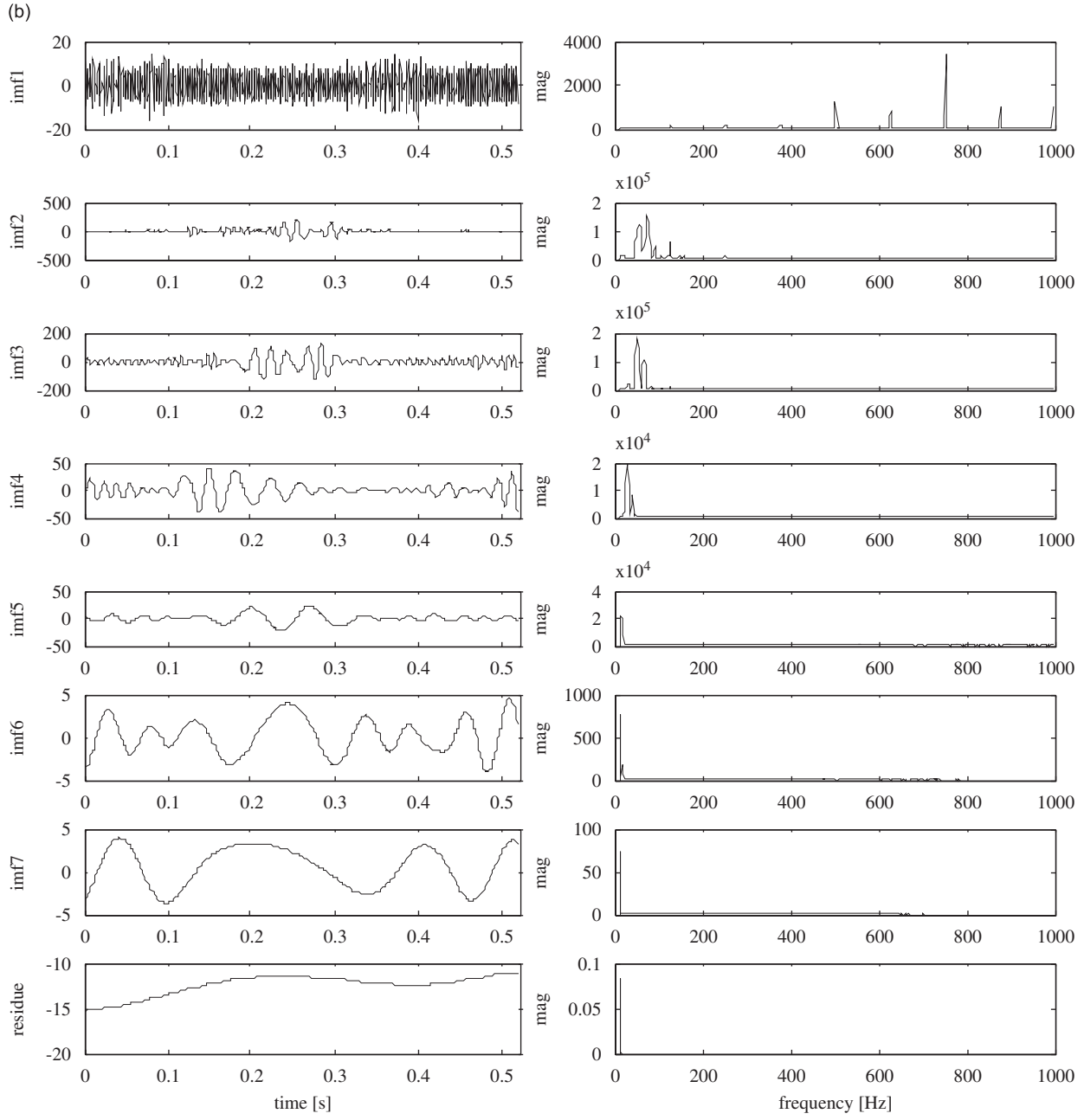

Fig. 13. (*Continued*)

Xingjiang Petroleum-Chemical Plant, and ZhenHai Oil Refinery in China. The mean values of all criteria obtained in this investigation are listed in Table 2. From Table 2, it is found that

- R_l, R_o, and R_u discriminate the machine running conditions roughly into four categories, as listed in Table 3.
- Criterion F correctly describes the smoothness of the shaft orbit. Its value is approximately 1 when the shaft runs normally. The significant divergence of F from 1 indicates the presence of a machine fault.

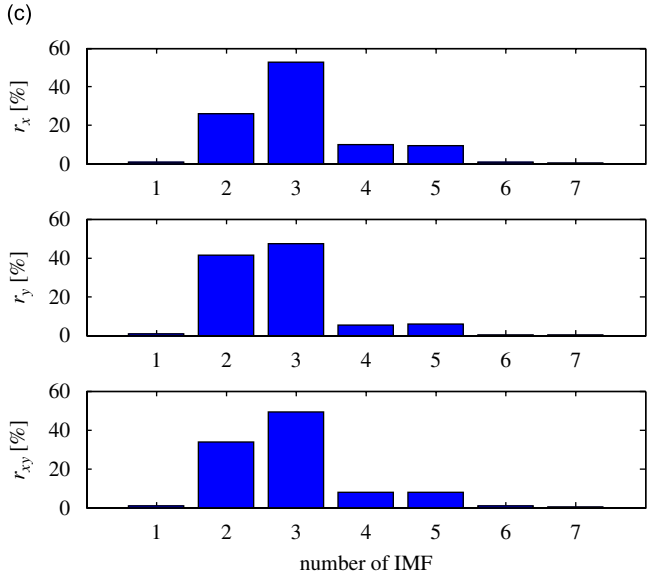

Fig. 13. (*Continued*)

- Criterion s_1 is a sensitive indicator of the stability of the shaft vibration in the bearing housing. In the presence of a part-loosening or rotor-to-stator rubbing fault, the shaft vibrates significantly in the bearing housing, which is characterized by a large s_1.
- Criterion s_2 measures the symmetric property of the shaft vibration in indifferent circumferential directions. Its value increases with the presence of a fault. Most interestingly, s_2 is so sensitive to the shaft health that it gives a strong response to the presence of an incipient transverse crack.
- Abnormal changes of machine condition affect the congruity and the harmonization of shaft vibration. Criterion s_3 reflects this phenomenon. From Table 2, it can be seen that both an increase and decrease of s_3 indicate a modification to the machine condition.
- Criteria s_4 and s_5 measure the variation of shaft central position with respect to the bearing housing. Large values of s_4 and s_5 indicate big fluctuations of the shaft axis. Table 2 reveals that part-loosening and rotor-to-stator rubbing faults are typically characterized by large s_4 and s_5.

From above observations, it can be concluded that the proposed mathematical criteria provide an effective assessment of machine running condition. However, it is worthy to note that all these mathematical criteria have not considered fault severity. So, in practice, better condition monitoring may be achieved if they are used in combination with trend analysis. With regard to the trend analysis for machine condition monitoring, the interested readers may refer to Refs. [28,29].

5. Conclusions

An adaptive technique is developed in the paper using the EMD approach to interpret shaft vibration signals collected from large rotating machines. Both the theoretical definition of the proposed technique and a number of mathematical criteria proposed for quantitative assessment of machine condition are described in detail, followed by verifications on practical data. From the work, the following conclusions have been reached:

- In comparison with the traditional FT approach, the EMD technique gives a more realistic and vivid image of transient shaft vibration attribute to the EMD does not involve any artificial transform. In particular, the TSO constructed by using the 'purified' principal IMFs clarifies potential misinterpretations of machine condition and leads to a more reliable machine fault diagnosis.

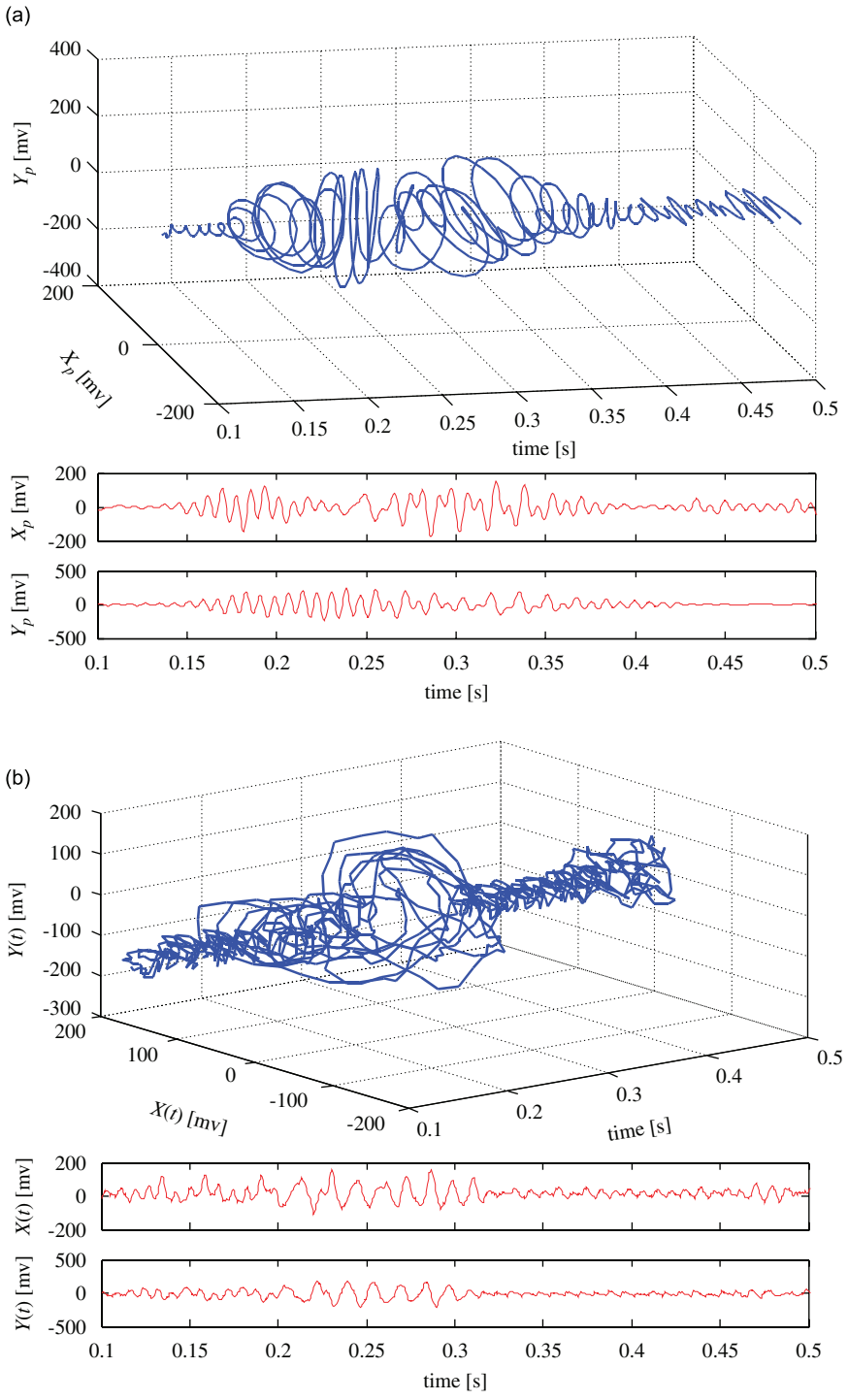

Fig. 14. The TSO in the presence of fluid excitation fault: (a) TSO by the EMD-based approach and (b) TSO by the original shaft vibration signals.

- In comparison with the WT approach, the EMD technique has a higher algorithmic efficiency. Therefore, it allows observation of longer term transient shaft vibrations. This is helpful for improving the reliability of machine condition assessment and diagnosis. In addition, it has been shown that the proposed technique

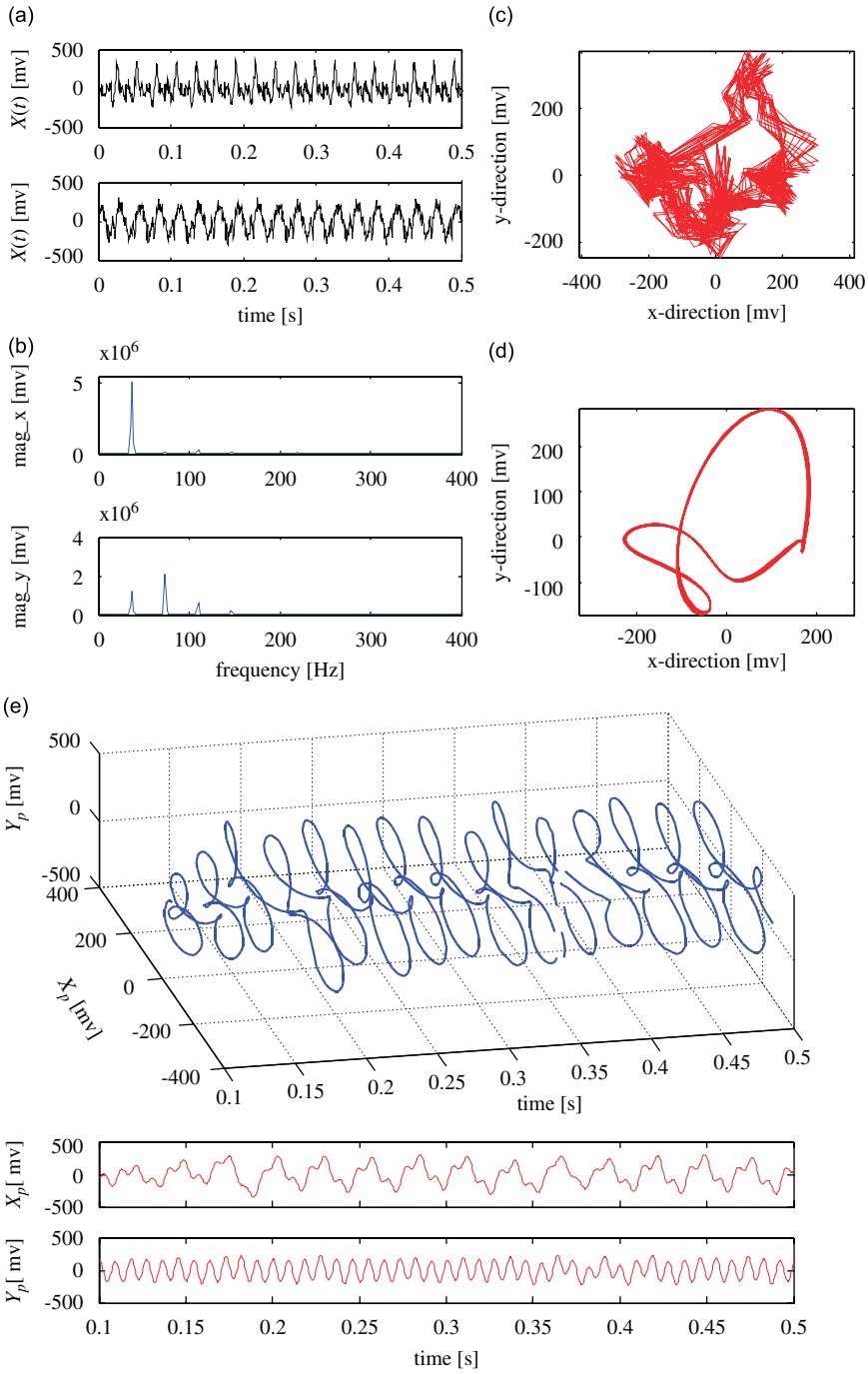

Fig. 15. The signals and the TSO in the presence of rotor-to-stator rubbing: (a) time-waveforms of the signals, (b) FFT spectra of the signals, (c) original shaft orbit, (d) purified shaft orbit derived by using the HRS, and (e) the TSO.

exhibits machine fault symptoms more satisfactorily than the WT because EMD minimizes the energy leakage problems in the vicinity of frequencies of interest.

- The mathematical criteria derived from the IMFs and the TSO possess exact physical significances. With their use the running condition of the shaft can be correctly assessed and the type of the fault can be

Table 2
Mean values of the criteria proposed in this investigation.

Running conditions of the shaft	Criteria								
	R_l	R_o	R_u	F	s_1	s_2	s_3	s_4	s_5
Coupling misalignment	0.0595	0.3234	0.6171	1.9774	11.9921	0.0656	3.3033	1.2192	0.0000
Part loosening	0.7016	0.0000	0.2984	8.4567	200.0732	0.0559	0.1738	100.9709	1.3256
Rotor-to-stator rubbing	0.0000	0.5519	0.4481	6.7089	132.5925	0.0638	2.7678	5.7744	0.0001
Fluid excitation	0.6268	0.3732	0.0000	3.9009	41.4020	0.0613	4.6189	2.2759	0.0047
Oil whirl	0.4729	0.5271	0.0000	1.8307	5.6073	0.0995	3.9507	0.0369	0.0433
Incipient transverse crack	0.0000	1.0000	0.0000	0.3718	32.4476	0.0147	3.3266	0.9048	0.0000
Normal rotor	0.0000	1.0000	0.0000	0.9990	0.0000	0.0000	2.6558	0.0000	0.0000

Table 3
Machine running conditions classified by R_l, R_o and R_u.

Category	Features	Possible conditions
1	$R_o \approx 1$, $R_l \approx R_u \approx 0$	Normal condition, rotor unbalance, the rotor with incipient transverse crack, and bent shaft
2	$R_u \approx 0$ but with large R_l and R_o	The faults characterized by low frequency vibration, such as fluid excitation, oil whirl, surge and the rotor with slight part loosening fault
3	$R_o \approx 0$ but with large R_l and smaller R_u	The faults characterized by both high and low frequency vibrations. It is often observed when serious part loosening fault happens
4	$R_l \approx 0$ but with large R_u and R_o	The faults characterized by high frequency vibration. For example, rotor-to-stator rubbing, coupling misalignment, the rotor with a big size of transverse crack

distinguished. It is anticipated that better condition monitoring can be achieved if these criteria are used in combination with trend analysis.

In summary, the proposed technique provides an effective tool for interpreting the nonlinear/non-stationary shaft vibrations in large rotating machines.

Acknowledgment

The latter part of this work was funded by the EPSRC Supergen Wind Energy Technologies Consortium, EP/D034566/1. The authors are grateful to the editor and anonymous referees for valuable comments. In the meantime, the experimental support from Shijiazhuang Petroleum Plant, Xingjiang Petroleum-Chemical Plant, ZhenHai Oil Refinery in China and the Research Institute of Diagnostics and Cybernetics in Xian Jiaotong University are gratefully acknowledged.

References

[1] D.F. Shi, W.J. Wang, P.J. Unsworth, L.S. Qu, Purification and feature extraction of shaft orbits for diagnosing large rotating machinery, *Journal of Sound and Vibration* 279 (2005) 581–600.
[2] S.M. Li, Harmonic wavelet packets method and used on accurate obtaining the orbit of rotor sub-frequency signal, *Chinese Journal of Mechanical Engineering* 9 (2004) 133–137.
[3] S.Q. Zhang, C.X. Wei, Z.P. Deng, The symptom extraction of axis orbit in fault diagnosis of hydropower generating units, *Journal of Huazhong University of Science and Technology (Nature Science)* 31 (4) (2003) 51–53.
[4] Y. Chen, Rotor orbit purification and its automatic identification, *Journal of Wuhan University of Technology (Transportation Science & Engineering)* 27 (6) (2003) 878–881.
[5] Z. Peng, Y. He, Z. Chen, F. Chu, Identification of the shaft orbit for rotating machines using wavelet modulus maxima, *Mechanical Systems and Signal Processing* 16 (4) (2002) 623–635.
[6] L.S. Qu, X. Liu, G. Peyronne, Y.D. Chen, The Holospectrum—a new method for rotor surveillance and diagnosis, *Mechanical Systems and Signal Processing* 3 (3) (1989) 255–267.

[7] Y.D. Chen, R. Du, L.S. Qu, Fault features of large machinery and diagnosis using sensor fusion, *Journal of Sound and Vibration* 188 (2) (1995) 227–242.
[8] W.X. Yang, L.S. Qu, J.S. Jiang, Study on the diagnostic features of a rotor with a transverse crack, *Insight (UK)* 43 (8) (2001) 537–545.
[9] W.X. Yang, X.M. Ren, J.S. Jiang, Survey on a few factors influencing the transient vibration behaviour of rotors, *Insight (UK)* 42 (8) (2000) 520–524.
[10] D.F. Shi, L.S. QU, M. Bao, Instantaneous purified orbit: a new tool for analysis non-stationary vibration of rotor system, *International Journal of Rotating Machinery* 7 (2001) 105–115.
[11] P.W. Tse, W.X. Yang, H.Y. Tam, Machine fault diagnosis through an effective exact wavelet analysis, *Journal of Sound and Vibration* 277 (2004) 1005–1024.
[12] Z.K. Peng, M.R. Jackson, J.A. Rongong, F.L. Chu, R.M. Parkin, On the energy leakage of discrete wavelet transform, *Mechanical Systems and Signal Processing* (2008), in press.
[13] W.X. Yang, A natural way for improving the accuracy of the continuous wavelet transforms, *Journal of Sound and Vibration* 306 (2007) 928–939.
[14] D.E. Newland, Ridge and phase identification in the frequency analysis of transient signals by harmonic wavelets, *Journal of Vibration and Acoustics—Transactions of the ASME* 121 (1999) 149–155.
[15] N.E. Huang, S. Zheng, S.R. Long, M.C. Wu, H.H. Shih, Q.A. Zheng, N.C. Yen, C.C. Tung, H.H. Liu, The empirical mode decomposition and the Hilbert spectrum for nonlinear and non-stationary time series analysis, *Proceedings of the Royal Society of London A* 454 (1998) 903–995.
[16] N.E. Huang, Z. Shen, S.R. Long, A new view of non-linear water waves: the Hilbert spectrum, *Annual Review of Fluid Mechanics* 31 (1999) 417–457.
[17] Q.H. Du, S.N. Yang, Application of the EMD method in the vibration analysis of ball bearings, *Mechanical Systems and Signal Processing* 21 (2007) 2634–2644.
[18] Q. Du, S. Yang, Improvement of the EMD method and applications in defect diagnosis of ball bearings, *Measurement Science & Technology* 17 (2006) 2355–2361.
[19] B. Liu, S. Riemenschneider, Y. Xu, Gearbox fault diagnosis using empirical mode decomposition and Hilbert spectrum, *Mechanical Systems and Signal Processing* 20 (2006) 718–734.
[20] Y. Yang, D.J. Yu, J.S. Cheng, A roller bearing fault diagnosis method based on EMD energy entropy and ANN, *Journal of Sound and Vibration* 294 (2006) 269–277.
[21] J.S. Cheng, D.J. Yu, Y. Yang, A fault diagnosis approach for roller bearings based on EMD method and AR model, *Mechanical Systems and Signal Processing* 20 (2006) 350–362.
[22] K.J. Guo, X.G. Zhang, H.G. Li, G. Meng, Application of EMD method to friction signal processing, *Mechanical Systems and Signal Processing* 22 (2008) 248–259.
[23] F.J. Wu, L.S. Qu, An improved method for restraining the end effect in empirical mode decomposition and its applications to the fault diagnosis of large rotating machinery, *Journal of Sound and Vibration* 314 (2008) 586–602.
[24] Y.S. Zhang, J.W. Liang, J.X. Hu, The processing of end effects in EMD method by autoregressive model, *Progresses in Nature Science* 13 (2003) 1054–1059.
[25] Y.J. Deng, W. Wang, Boundary processing technique in EMD method and Hilbert transform, *Chinese Science Bulletin* 46 (2001) 257–263.
[26] Z.K. Peng, P.W. Tse, F.L. Chu, An improved Hilbert–Huang transform and its applications for vibration signals analysis, *Journal of Sound and Vibration* 286 (2005) 187–205.
[27] Z.K. Peng, P.W. Tse, F.L. Chu, A comparison study of improved Hilbert–Huang transform and wavelet transform: application to fault diagnosis for rolling bearing, *Mechanical Systems and Signal Processing* 19 (2005) 974–988.
[28] J.D. Jiang, J. Chen, L.S. Qu, The application of correlation dimension in gearbox condition monitoring, *Journal of Sound and Vibration* 223 (1999) 529–541.
[29] W.J. Wang, Z.T. Wu, J. Chen, Fault identification in rotating machinery using the correlation dimension and bispectra, *Nonlinear Dynamics* 25 (2001) 383–393.